Anomalous Collective Dynamics of Autochemotactic Populations

Jasper van der Kolk,[1,*] Florian Raßhofer,[1,*] Richard Swiderski,[1,*] Astik Haldar,[2] Abhik Basu,[2] and Erwin Frey[1,3,†]
[1]Arnold Sommerfeld Center for Theoretical Physics and Center for NanoScience, Department of Physics, Ludwig-Maximilians-Universität München, Theresienstraße 37, D-80333 Munich, Germany
[2]Theory Division, Saha Institute of Nuclear Physics, HBNI, 1/AF Bidhannagar, Calcutta 700 064, West Bengal, India
[3]Max Planck School Matter to Life, Hofgartenstraße 8, 80539 Munich, Germany

(Received 23 December 2021; revised 20 January 2023; accepted 21 June 2023; published 23 August 2023)

While the role of local interactions in nonequilibrium phase transitions is well studied, a fundamental understanding of the effects of long-range interactions is lacking. We study the critical dynamics of reproducing agents subject to autochemotactic interactions and limited resources. A renormalization group analysis reveals distinct scaling regimes for fast (attractive or repulsive) interactions; for slow signal transduction, the dynamics is dominated by a diffusive fixed point. Furthermore, we present a correction to the Keller-Segel nonlinearity emerging close to the extinction threshold and a novel nonlinear mechanism that stabilizes the continuous transition against the emergence of a characteristic length scale due to a chemotactic collapse.

DOI: 10.1103/PhysRevLett.131.088201

Nonequilibrium phase transitions encompass a broad class of systems, including absorbing-state phase transitions [1,2], roughening transitions [3,4], and ordering transitions in active matter [5,6]. Most theoretical studies of these paradigmatic model systems focus on the role of local interactions. However, in addition to short-ranged interactions, several biological and synthetic systems exhibit many-body long-range interactions between agents [7]. For example, the social amoeba *Dictyostelium discoideum* uses chemical signaling and chemotaxis to control aggregation under harsh conditions [8], signaling molecules mediate intercellular communication in microbial populations [9], and microrobots and robotic fish use infrared, electrical, and acoustic signals to communicate [10].

Studying long-ranged interactions has a long-standing history in the context of equilibrium continuous phase transitions [11–13]. Their nonequilibrium counterparts are, however, less well explored. Most attention has been paid to systems where the long-rangedness results from Lévy-flight-like motion, nonlocal effects due to an underlying network architecture, or spatially dependent reaction rates [14–17]. There, the additional interactions may lead to a new universality class [14,16] or change the nature of the phase transition [17]. Here, we are interested in the role of long-range chemical signaling on classical models of population dynamics.

For this purpose, we consider agents emitting a signal in the form of a chemical substance which spreads by diffusion and can be sensed by other agents that respond by adapting their direction of motion, a process known as *chemotaxis*. The dynamics of such populations has been analyzed in terms of drift-diffusion models for the agent density coupled to a chemical field, termed *Keller-Segel* (KS) models [18–20]. These studies have identified a plethora of different phenomena—ranging from aggregation [21,22] to the formation of complex patterns [19,23–25]. While the role of thermal fluctuations [26,27] and fluctuations around a constant background density [28,29] have been investigated, the role of large-scale demographic noise—which is particularly important close to the extinction threshold [1,2,30]—remains largely unexplored. In this Letter, we investigate how long-ranged chemical signaling affects the collective behavior of a population consisting of a single type of reproducing agents close to extinction.

We consider a generic model of a population of diffusing cells (agents) and chemicals in terms of two fluctuating density fields $\rho(\mathbf{x},t)$ and $c(\mathbf{x},t)$. The population dynamics is assumed to follow logistic growth; i.e., cells proliferate at a rate μ, die at a rate λ, and resource availability limits population growth to a finite carrying capacity. In addition, we consider the effect of an *autochemotactic interaction*, where each cell is capable of responding to a chemical signal while simultaneously sourcing it with strength α [31,32]. We are interested in an effective, hydrodynamic description of this system, valid on macroscopic scales and in the presence of demographic noise. The corresponding Langevin equations are

$$\frac{d\rho}{dt} = (D_\rho \nabla^2 + \theta)\rho - \gamma\rho^2 + \sqrt{2\Lambda\rho}\xi + I[\rho, \nabla c], \quad (1)$$

$$\frac{dc}{dt} = (D_c \nabla^2 - \lambda_c)c + \alpha\rho, \quad (2)$$

where $\theta = \mu - \lambda$ is the net growth rate, θ/γ the carrying capacity, λ_c the degradation rate of the signaling molecules, and $D_{\rho,c}$ are the diffusion constants. The macroscopically relevant noise is multiplicative with amplitude $2\Lambda\rho(\boldsymbol{x}, t)$ and Gaussian white noise $\xi(\boldsymbol{x}, t)$. Higher-order nonlinearities and other noise terms are irrelevant close to the absorbing state [33]. Without the additional interaction $I[\rho, \nabla c]$, Eq. (1) corresponds to the noisy *Fisher-Kolmogorov* equation [53,54], whose universal properties fall into the universality class of *directed percolation* (DP) [1,2].

The interaction term $I[\rho, \nabla c]$—which we assume to depend only on gradients in c [33]—accounts for the directed motion of cells along chemical gradients. Its form depends not only on cellular details, but also on the level of coarse graining. In particular, the absence of global mass conservation in the population dynamics allows for a nonconservative effective interaction.

At mean-field level, the dynamics exhibits two length scales, a diffusion length of the agents $\xi_\rho = \sqrt{D_\rho/|\theta|}$ and of the chemicals $\xi_c = \sqrt{D_c/\lambda_c}$. The latter is linked to the interaction range, since λ_c inhibits signal transduction over long distances. For long-ranged chemotactic interactions ($\xi_c \to \infty$, see Appendix A) [33], the only relevant scale is ξ_ρ. Below this scale, demographic processes play only a minor role and the chemotactic interaction can be formulated in terms of a conserved current $I[\rho, \nabla c] = \nabla \boldsymbol{J}$, where $\boldsymbol{J} = \chi[\rho, \nabla c]\rho\nabla c$ and the sensitivity function $\chi[\rho, \nabla c]$ encodes details of the sensing process [19,55,56].

However, close to the extinction threshold, the system is dominated by a divergent correlation length $\xi > \xi_\rho$ and strongly enhanced fluctuations. Furthermore, coarse graining to large scales inevitably "mixes" the effects of chemotaxis and birth-death processes. Whereas the net production by the linear birth-death term is independent of the density distribution, the net degradation due to the growth-limiting term is enhanced by density fluctuations. Thus, the evolution of the total mass is coupled to the chemotactic interaction by the interplay of resource limitation and chemotactic drift, which alters the dynamics of density fluctuations. Therefore, an explicit coarse-graining procedure is needed to determine all the relevant contributions. This is achieved by a *renormalization group* (RG) analysis (see Ref. [33]), which reveals that close to the extinction threshold the effective chemotactic interaction, correctly accounting for birth-death processes, is given by

$$I[\rho, \nabla c] = \chi_1 \nabla(\rho\nabla c) + (\chi_2 - \chi_1)\rho\nabla^2 c. \quad (3)$$

It consists of a conservative interaction—the classical KS [18] nonlinearity—and an additional nonconservative term.

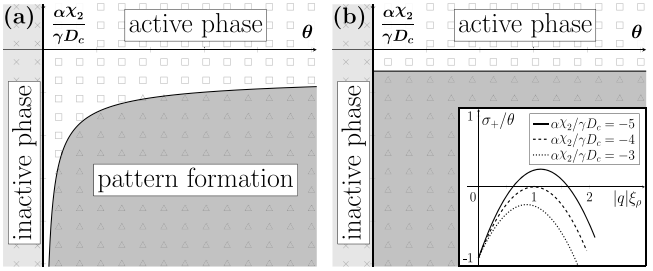

FIG. 1. Mean-field phase diagrams of the auto-chemotactic model for $\lambda_c = 0.1$ (a) and $\lambda_c = 0$ (b) with an inactive phase (light gray), an active phase (white), and a pattern formation regime (dark gray). The boundary between the active phase and the pattern formation regime is given by Eq. (4). The states obtained from finite element simulations in one spatial dimension for $D = 0.1$, $\gamma = D_c = 1$, $\alpha = 5$, $\theta \in [-0.2, 1]$ and $\chi_1 = \chi_2 \in [-2, 0.4]$ are marked by crosses (absorbing state), squares (active state) and triangles (inhomogeneous), respectively. The inset shows the largest eigenvalue of the system at $\lambda_c = \theta$ and $D_c = D_\rho$.

A dimensional analysis shows that all other contributions are irrelevant at the pertinent length scales [33]. Importantly, Eq. (3) does not imply that the chemotactic interaction explicitly breaks particle number conservation. Rather, it accounts for the fact that close to the extinction threshold the interplay between strong density fluctuations, chemotactic drift, and population dynamics requires an *effective* description of the form (3). Conversely, if fluctuation corrections are weak, i.e., far away from the extinction threshold, a conserved current yields the proper description.

To analyze Eqs. (1) and (2), we first neglect the noise term and study the resulting mean-field equations. They yield two homogeneous stationary solutions: the *absorbing state* $\rho_0 = c_0 = 0$ corresponding to the *inactive phase* and a state corresponding to the *active phase* with the agent density equal to the carrying capacity: $\rho_1 = \theta/\gamma$ and $c_1 = \alpha\rho_1/\lambda_c$. From a linear stability analysis of these homogeneous states, one infers that there are three distinct phases (Fig. 1). For $\theta < 0$, only the absorbing state is stable. In contrast, the homogeneous active state is stable for $\theta > 0$ and

$$\chi_2 > -\frac{\gamma D_c}{\alpha}\left(1 + \frac{\lambda_c D_\rho}{\theta D_c} + 2\sqrt{\frac{\lambda_c D_\rho}{\theta D_c}}\right). \quad (4)$$

In the case of $\theta > 0$ and χ_2 below this threshold, however, both homogeneous solutions are unstable against spatial perturbations. This Turing-type [57] instability indicates the onset of pattern formation [24,25], as explicitly confirmed by numerical simulations shown in Fig. 1.

At $\theta = 0$, one finds a transcritical bifurcation, indicating a continuous, absorbing-state phase transition with θ acting as the control parameter. Close to the extinction threshold ($\theta \to 0$) and for long-ranged interactions ($\xi_c \to \infty$), the system becomes intrinsically scale invariant. In particular,

the correlation length of density fluctuations should diverge as $\xi \propto \theta^{-\nu}$, and, for a cell cluster emerging from a single seed, its mean-squared radius and survival probability at criticality should scale as $\langle R^2 \rangle(t) \propto t^{2/z}$ and $P(t) \propto t^{-\delta}$, respectively [1,2]. The mean-field critical exponents are given by $\nu = 0.5$, $z = 2$, and $\delta = d/4$. By dimensional analysis, one identifies the following effective parameters:

$$u = \frac{\gamma \Lambda}{32\pi^2 D_\rho^2}, \quad g_{1,2} = \frac{\alpha \chi_{1,2} \Lambda}{32\pi^2 D_\rho^2 D_c}, \quad w = \frac{D_c}{D_c + D_\rho}. \tag{5}$$

In addition to the DP coupling u (representing resource limitation), two new chemotactic couplings g_1 and g_2 emerge. The parameter w measures the time delay in the chemotactic interaction due to the finite diffusion speed of the signaling molecules. Employing field theoretical RG and a systematic perturbation expansion around the upper critical dimension $d_c = 4$, we derive the flow equations [33]

$$\mu \frac{du}{d\mu} = -\epsilon u + f_1(u, g_{1,2}, w), \tag{6a}$$

$$\mu \frac{dg_{1,2}}{d\mu} = -\epsilon g_{1,2} + f_{2,3}(u, g_{1,2}, w), \tag{6b}$$

$$\mu \frac{dw}{d\mu} = -w(1-w) f_4(u, g_{1,2}, w). \tag{6c}$$

The flow functions f_1–f_4 contain all information about the dependence of the theory on the arbitrary momentum scale μ in $d = 4 - \varepsilon$ dimensions. Scale invariance is implied by the existence of IR-stable ($\mu \to 0$ stable) fixed points [30].

In contrast to previous studies [28], all calculations are performed by approaching the phase transition from the inactive phase, the full dynamics of the chemical concentration field are taken into account, and the limiting case of DP is correctly recovered.

Inspecting Eq. (6c), one observes that $w = 1$ is an invariant manifold of the RG flow. Moreover, systems where $w \lesssim 1$ only slowly evolve away from this hyperplane. Therefore, we first focus on this *quasistatic* limit of infinitely fast diffusing chemicals [33].

We begin by investigating the case of a classical KS interaction. This implies starting the RG coarse graining at a scale where the chemotactic nonlinearities are equal, i.e., $g_1 = g_2 = g_0$ (gray plane in Fig. 2). In addition to the anticipated Gaussian and DP fixed points, the RG flow exhibits a stable fixed point (CA) and a stable fixed line (CR) (Fig. 2). They represent two different types of scale-invariant dynamics, corresponding to chemoattractive (CA) and chemorepellent (CR) systems. Only if $g_0 = 0$ does the flow reach the DP fixed point, which is unstable under the inclusion of chemotaxis, highlighting the importance of long-ranged interaction for the agents' critical behavior. Furthermore, irrespective of the sign of the interaction, the flow leaves the plane of KS interactions and terminates in either the stable subdiffusive CA fixed point ($z = 2 + \epsilon/18$) for chemoattraction ($g_0 < 0$) or the stable superdiffusive CR fixed line ($z = 2 - \epsilon/2$) for chemorepulsion ($g_0 > 0$).

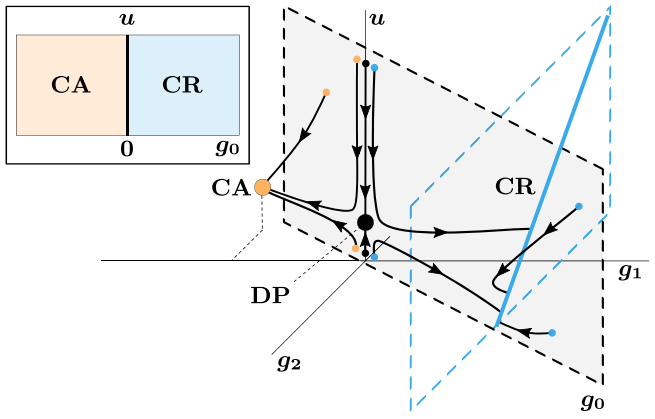

FIG. 2. Schematic flow lines at $w = 1$ for initial conditions sampled from the KS plane $g_1 = g_2 = g_0$ (gray plane). The basins of attraction for the DP (black), CA (orange), and CR (blue) fixed point are shown in the inset. In units of ε, the fixed point values (u, g_1, g_2) are $(1/12, 0, 0)$, $(1/9, -1/3, -1/6)$, and $(-g_2/2, 1/2, g_2)$, respectively. All flow lines starting from $g_0 \neq 0$ leave the KS plane.

We conclude that accounting for long-range chemotactic interactions quantitatively changes the nature of the phase transition compared to DP, leading to two new universality classes of absorbing-state phase transitions. The values of the associated dynamical exponents z (Table I) match the expectation that chemorepellent agents accelerate and chemoattractant agents decelerate colony dispersal compared to DP.

Furthermore, the fact that all flow lines leave the $g_1 = g_2$ plane confirms that a KS interaction is not sufficient to model the universal dynamics near criticality. Fluctuation-generated terms are a generic phenomenon close to critical points [34,42]. Similarly, in our case, the nonconservative part of Eq. (3) is "generated" even if not included from the beginning, and the effective chemotactic interaction can, in general, not be given in terms of a conserved current. Consequently, close to criticality, $g_1 \neq g_2$ is of great physical interest. In particular, the question arises how the RG analysis relates to the mean-field analysis, which

TABLE I. Critical exponents up to first loop order for the four distinct fixed points.

	ν	z	δ
DP	$0.5 + \frac{\epsilon}{16}$	$2 - \frac{\epsilon}{12}$	$1 - \frac{\epsilon}{4}$
CA	$0.5 + \frac{\epsilon}{8}$	$2 + \frac{\epsilon}{18}$	$1 - \frac{5\epsilon}{6}$
CR	$0.5 + \frac{\epsilon}{8}$	$2 - \frac{\epsilon}{2}$	1
CP	$0.5 + 0.13\epsilon$	2	$1 - 0.93\epsilon$

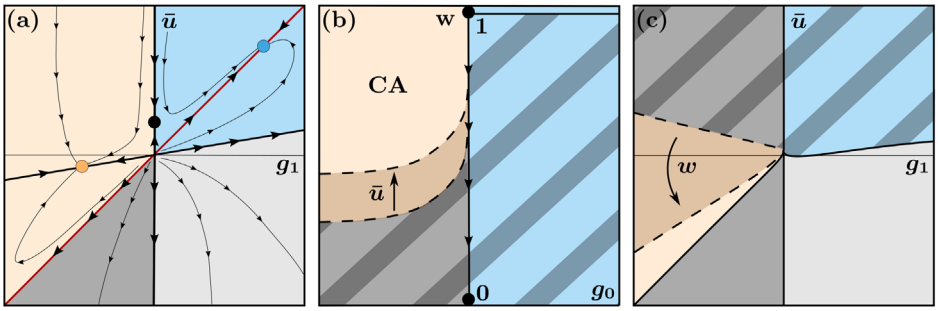

FIG. 3. Evolution of initial conditions sampled from different slices of the four-dimensional parameter space under the RG flow, which is classified into flow toward the CA fixed point (orange), the CR fixed line (blue), and four possibly different kinds of runaway flow (gray and striped areas). The striped areas indicate effects which are present only at $w < 1$. (a) Schematic flow lines in the $\bar{u} - g_1$ plane for $w = 1$ with three invariant manifolds $g_1 = 0$, $\bar{u} = g_1$, and $\bar{u} = g_1/6$ (bold lines). (b) Typical flow behaviors for KS-type models with $g_1 = g_2 = g_0$ at fixed u with DP fixed points at $w = 1$ (unstable) and $w = 0$ (stable). The separatrix (dashed line) introduced by the CP fixed point (not shown) is shifted by increasing u (darker orange region). The CR fixed line is stable only at $w = 1$. (c) Typical flow behaviors for $w < 1$ and u fixed. The influence of decreasing w on the basin of attraction of CA is indicated by dashed lines and the darker orange region. The phase boundaries in (b) and (c) were obtained by numerically solving the flow equations (6a)–(6c) [33].

identified a band of linearly unstable modes for $g_2 < -u$ (in the long-ranged limit).

Indeed, the RG flow equations can be rewritten as a set of only two equations for $\bar{u} = u + g_2$ and g_1: In the quasistatic limit, the solution of the resulting Poisson equation (see Appendix B) allows one to eliminate the chemical field, leading (among other terms) to an effective growth-limiting term with the shifted coupling constant $\bar{u} = u + g_2$ [33].

We find that the domains of attraction of the CA and CR fixed points are separated by an invariant manifold at $g_1 = 0$ [Fig. 3(a)], leading to two different types of dynamical scaling behaviors for $g_1 < 0$ and $g_1 > 0$, respectively. This further stresses the difference between the two chemotactic couplings: While the term $\sim g_2 \rho \boldsymbol{\nabla}^2 c$ can be absorbed into an effective growth-limiting term, only the nonlinearity $\sim g_1 \boldsymbol{\nabla}\rho\boldsymbol{\nabla} c$ qualitatively changes the RG flow. In addition to the separatrix at $g_1 = 0$, the RG flow is organized by the critical manifolds containing the CA and CR fixed points, given (to one-loop order) by the lines $\bar{u} = g_1/6$ and $\bar{u} = g_1$, respectively [Fig. 3(a)]. These lines are also the boundaries of the domains of attraction of the CA (orange) and CR (blue) fixed points, separating them from runaway flow.

Given that, in the long-ranged limit, the instability condition (4) simplifies to $\bar{u} < 0$, one might have anticipated runaway flow in this entire region. Strikingly, the RG analysis predicts scaling for $g_1 < \bar{u} < 0$, which seems contradictory at first. However, the linear stability analysis does not allow any conclusions about the steady state of the dynamics. Crucially, g_1 does not affect the linear dynamics but contributes only to nonlinear effects. In particular, it enters the following exact relation for the time evolution of the average mass (see Appendix C):

$$\frac{\Lambda(\partial_t\langle\bar{\rho}\rangle - \theta\langle\bar{\rho}\rangle)}{32\pi^2 D_\rho^2} = -u\langle\bar{\rho}^2\rangle + \frac{g_1 - \bar{u}}{|V|}\int_V \langle(\rho - \bar{\rho})^2\rangle, \quad (7)$$

where $\bar{\rho}$ indicates a spatial and $\langle\cdot\rangle$ an ensemble average with respect to the noise ξ. Equation (7) implies that, depending on the sign of $g_1 - \bar{u}$, fluctuations drive the system either toward or away from the absorbing state. It applies to the dynamics both above and below the absorbing-state phase transition and especially when approaching the phase transition at $\theta, \bar{\rho} \to 0$. This rationalizes why for $\bar{u} - g_1 > 0$ (including all KS models) nonlinear effects combined with demographic noise lead to a continuous absorbing-state phase transition, despite the band of linear unstable modes for $\bar{u} < 0$. In contrast, for $g_1 > 0$, the system is attracted by the CR fixed point for $\bar{u} > g_1/6$ and exhibits runaway flow when $\bar{u} < g_1/6$ [Fig. 3(a)]. The region $0 < \bar{u} < g_1$ is particularly interesting: Eq. (7) implies that the linear stability of the spatially uniform, active state is counteracted by a nonlinear term $(\sim g_1 - \bar{u})$ disfavoring a homogeneous state. Our RG analysis indicates that the antagonism between these two effects leads to flow toward the CR fixed point in the regime $g_1 > \bar{u} > g_1/6$ but to runaway flow for $\bar{u} < g_1/6$. Since the nonlinear instability is dominant in the latter regime, the observed runaway flow is possibly indicative of a fluctuation-driven first-order transition.

The agents' active motion can result in an effective diffusion constant D_ρ of similar magnitude as D_c [31,58,59]. Therefore, it is crucial to study the case $w \approx 1$. In this case, the full flow equations (6a)–(6c) exhibit an additional fixed point of mixed stability we call the critical fixed point (CP) at $(u, g_1, g_2, w) = (0.08\varepsilon, -0.45\varepsilon, -0.16\varepsilon, 0.64)$ and a second DP fixed point at $w = 0$. Our RG analysis shows that the CP fixed point has a dynamic critical exponent $z = 2$ to all loop orders [33], implying purely diffusive dynamics, akin to the critical fixed point characterizing the roughening transition of the Kardar-Parisi-Zhang (KPZ) equation [4,60,61]. As before, we first consider the case of $g_1 = g_2 = g_0$; the resulting basins of attraction for the various fixed points are depicted in Fig. 3(b). All points located on

the invariant manifold $g_0 = 0$ flow toward the second DP fixed point at $w = 0$. Since the CP fixed point is located at $w < 1$ and unstable in the w direction, it separates the parameter space $g_0 < 0$ into two parts. Points above this separatrix flow to CA, whereas below it the system exhibits a new type of runaway flow (striped dark gray). In contrast to CA, the basin of attraction of CR does not extend to $w < 1$. As pointed out above, a chemorepellent implies superdiffusive motion ($z < 2$), equivalent to $\partial_\mu w < 0$ near the fixed line (CR). This renders the fixed line unstable in the w direction. However, in the emerging runaway region (striped blue), the projection of the fixed line to $w < 1$ is still a strong attractor, which separates it from other regions of runaway flow [Figs. 3(b) and 3(c)]. The typical shape of the phase diagram for general g_1 and g_2, at fixed values of u and w, is shown in Fig. 3(c). It features all four, possibly different, kinds of runaway flow and bears a strong resemblance to Fig. 3(a).

Altogether, the analyzed model reveals a correction to the well-known Keller-Segel nonlinearity in the presence of large fluctuations and exhibits a rich phase diagram with two new absorbing-state phase transitions and various types of runaway regions. The emergence of fixed points associated to either a chemoattractant or -repellent demonstrates the relevance of autochemotactic interactions for the collective behavior of cells at their extinction threshold. In particular, they highlight the impact of chemotactic signaling for the survival probability and spreading velocity of single colonies (Table I). For $w = 1$, we have presented a possible mechanism by which the runaway flow found in Fig. 3(a) can be related to a fluctuation-induced first-order transition [cf. Eq. (7)].

Furthermore, the emergence of the CP fixed point not only gives rise to an unexpected type of purely diffusive scaling behavior, it also highlights the importance of the time delay introduced by the finite diffusion speed of the signaling substance. The reminiscence of the CP fixed point to the critical fixed point describing the roughening transition of the KPZ equation suggests the intriguing scenario of a strong coupling fixed point below the separatrix.

Naturally, the multitude of theoretical predictions presented calls for a numerical study. Additionally, we hope that our work will stimulate nonperturbative approaches [35,36] that help to unravel the observed anomalous dynamics. From a broader perspective, our results suggest that by combining known universality classes of nonequilibrium population dynamics [2,30] with various types of autochemotactic feedbacks, a broad class of novel scale-invariant dynamics could be discovered.

This work was funded by the Deutsche Forschungsgemeinschaft (DFG, German Research Foundation) through the Collaborative Research Center SFB 1032—Project-ID No. 201269156—and the Excellence Cluster ORIGINS under Germany's Excellence Strategy—EXC-2094–390783311. Abhik Basu thanks the SERB, DST (India) for partial financial support through the MATRICS scheme (File No. MTR/2020/000406).

Appendix A: Long-ranged limit.—Since scale invariance can be observed only if no length scale is introduced by the chemotactic interaction, the long-ranged limit $\lambda_c \to 0$ is of particular interest. However, simply inserting $\lambda_c = 0$ into Eqs. (1) and (2) leads to a divergent chemical density and a steady state condition $\rho_1 = -D_c \nabla^2 c_1(\boldsymbol{x})/\alpha$. Thus, there would no longer be a homogeneous steady state for the chemical density, which leads to an unphysical shift to the homogeneous steady state density $\rho_1 = \theta/(\gamma + \alpha\chi_2/D_c)$ of the agents. This deviates from the actual carrying capacity θ/γ and shows that one needs to take into account the "charge-neutral" chemical density

$$\tilde{c}(\boldsymbol{x}, t) = c(\boldsymbol{x}, t) - \alpha \int_0^t dt' \bar{\rho}(t'), \tag{A1}$$

where we subtracted the homogeneous, albeit time-dependent average production of the signaling molecule with $\bar{\rho}(t)$ denoting the spatial average of ρ at time t.

Importantly, this homogeneous shift does not alter the dynamics of ρ. However, the evolution of the charge-neutral chemical density is now given by

$$\frac{d\tilde{c}}{dt} = D_c \nabla^2 \tilde{c} + \alpha(\rho - \bar{\rho}), \tag{A2}$$

with no overall net production, i.e.,

$$\frac{d}{dt} \int_V \tilde{c} = 0. \tag{A3}$$

More details on this limit are provided in Supplemental Material [33].

Appendix B: Quasistatic limit.—Another important limit is the so-called *quasistatic limit*, where $D_c/D_\rho \to \infty$ and the chemical field, thus, instantly adjusts to changes in the density field ρ. Assuming that α/D_c remains finite [21], Eq. (A2) leads to the Poisson equation

$$\nabla^2 \tilde{c}(\boldsymbol{x}, t) = -\frac{\alpha}{D_c}[\rho(\boldsymbol{x}, t) - \bar{\rho}(t)]. \tag{B1}$$

For more details, we refer to Supplemental Material [33].

Appendix C: Mass evolution.—One way to analyze the impact of different interactions is to study their effect on the time evolution of the average density $\langle \bar{\rho} \rangle$, where $\langle \cdot \rangle$ signifies an ensemble average with respect to the noise ξ. To derive this evolution, we first note that Eqs. (1) and (2) are Itô Langevin equations and, thus,

$$\int_V \langle \sqrt{2\Lambda\rho}\xi \rangle = \int_V \langle \sqrt{2\Lambda\rho} \rangle \langle \xi \rangle = 0. \tag{C1}$$

Furthermore, we split the agents' density into $\rho(\boldsymbol{x}, t) = \bar{\rho}(t) + \hat{\rho}(\boldsymbol{x}, t)$, integrate Eq. (1) over space, and insert

Eq. (B1). For the deterministic terms, this yields

$$\partial_t\bar{\rho} = \theta\bar{\rho} - \frac{1}{|V|}\int_V (\bar{\rho}+\hat{\rho})\left(\gamma(\bar{\rho}+\hat{\rho}) + \frac{\alpha(\chi_1+\chi_2)}{D_c}\hat{\rho}\right)$$
$$= \theta\bar{\rho} + \frac{32\pi^2 D_\rho^2}{\Lambda}\left(-u\bar{\rho}^2 + \frac{g_1-\bar{u}}{|V|}\int_V \hat{\rho}\right), \tag{C2}$$

where we used that $\int_V \hat{\rho} = 0$ and used the definitions (5) of the effective couplings, as well as $\bar{u} = u + g_2$. Taking the ensemble average of Eq. (C2) leads to the exact result of Eq. (7). This result highlights the difference between the linear growth term $\propto \theta$ and the nonlinearity $\propto \gamma$ modeling resource limitation. While the former contributes a distribution-independent term to Eq. (C2), the latter leads to a mass evolution which is dependent on the density profile. Thus, it is the resource limitation which makes the mass evolution susceptible to the influence of chemotaxis.

*These authors contributed equally to this work.
†Corresponding author.
frey@lmu.de

[1] H. Hinrichsen, Non-equilibrium critical phenomena and phase transitions into absorbing states, Adv. Phys. **49**, 815 (2000).
[2] H. K. Janssen and U. C. Täuber, The field theory approach to percolation processes, Ann. Phys. (Amsterdam) **315**, 147 (2005), special Issue.
[3] T. Halpin-Healy and Y. C. Zhang, Kinetic roughening phenomena, stochastic growth, directed polymers and all that. Aspects of multidisciplinary statistical mechanics, Phys. Rep. **254**, 215 (1995).
[4] M. Kardar, G. Parisi, and Y. C. Zhang, Dynamic Scaling of Growing Interfaces, Phys. Rev. Lett. **56**, 889 (1986).
[5] S. Ramaswamy, The mechanics and statistics of active matter, Annu. Rev. Condens. Matter Phys. **1**, 323 (2010).
[6] M. C. Marchetti, J. F. Joanny, S. Ramaswamy, T. B. Liverpool, J. Prost, M. Rao, and R. A. Simha, Hydrodynamics of soft active matter, Rev. Mod. Phys. **85**, 1143 (2013).
[7] A. Ziepke, I. Maryshev, I. S. Aranson, and Erwin Frey, Multi-scale organization in communicating active matter, Nat. Commun. **13**, 6727 (2022).
[8] C. A. Parent and P. N. Devreotes, A cell's sense of direction, Science **284**, 765 (1999).
[9] M. Bauer, J. Knebel, M. Lechner, P. Pickl, and E. Frey, Ecological feedback in quorum-sensing microbial populations can induce heterogeneous production of autoinducers, eLife **6**, 25773 (2017).
[10] R. K. Katzschmann, J. DelPreto, R. MacCurdy, and D. Rus, Exploration of underwater life with an acoustically controlled soft robotic fish, Sci. Rob. **3**, aar3449 (2018).
[11] M. E. Fisher, S. K. Ma, and B. G. Nickel, Critical Exponents for Long-Range Interactions, Phys. Rev. Lett. **29**, 917 (1972).
[12] E. Frey and F. Schwabl, Critical dynamics of magnets, Adv. Phys. **43**, 577 (1994).
[13] E. Bayong, H. T. Diep, and T. T. Truong, Phase transition in a general continuous Ising model with long-range interactions, J. Appl. Phys. **85**, 6088 (1999).
[14] H. K. Janssen, K. Oerding, F. van Wijland, and H. J. Hilhorst, Lévy-flight spreading of epidemic processes leading to percolating clusters, Eur. Phys. J. B **7**, 137 (1999).
[15] H. Hinrichsen, Non-equilibrium phase transitions with long-range interactions, J. Stat. Mech. (2007) P07006.
[16] C. Argolo, Y. Quintino, P. H. Barros, and M. L. Lyra, Vanishing order-parameter critical fluctuations of an absorbing-state transition driven by long-range interactions, Phys. Rev. E **87**, 032141 (2013).
[17] S. M. Reia and J. F. Fontanari, Effect of long-range interactions on the phase transition of Axelrod's model, Phys. Rev. E **94**, 052149 (2016).
[18] E. F. Keller and L. A. Segel, Model for chemotaxis, J. Theor. Biol. **30**, 225 (1971).
[19] T. Hillen and K. J. Painter, A user's guide to PDE models for chemotaxis, J. Math. Biol. **58**, 183 (2008).
[20] M. J. Tindall, P. K. Maini, S. L. Porter, and J. P. Armitage, Overview of mathematical approaches used to model bacterial chemotaxis II: Bacterial populations, Bull. Math. Biol. **70**, 1570 (2008).
[21] W. Jäger and S. Luckhaus, On explosions of solutions to a system of partial differential equations modelling chemotaxis, Trans. Am. Math. Soc. **329**, 819 (1992).
[22] M. A. Herrero and J. J. L. Velázquez, A blow-up mechanism for a chemotaxis model, Ann. Sc. Norm. Super. Pisa-Classe Sci. **24**, 633 (1997).
[23] R. Tyson, S. R. Lubkin, and J. D. Murray, Model and analysis of chemotactic bacterial patterns in a liquid medium, J. Math. Biol. **38**, 359 (1999).
[24] J. I. Tello and M. Winkler, A chemotaxis system with logistic source, Commun. Partial Differ. Equations **32**, 849 (2007).
[25] L. Jin, Q. Wang, and Z. Zhang, Pattern formation in Keller–Segel chemotaxis models with logistic growth, Int. J. Bifurcation Chaos Appl. Sci. Eng. **26**, 1650033 (2016).
[26] P. H. Chavanis, A stochastic Keller-Segel model of chemotaxis, Commun. Nonlinear Sci. Numer. Simul. **15**, 60 (2008).
[27] T. J. Newman and R. Grima, Many-body theory of chemotactic cell-cell interactions, Phys. Rev. E **70**, 051916 (2004).
[28] A. Gelimson and R. Golestanian, Collective Dynamics of Dividing Chemotactic Cells, Phys. Rev. Lett. **114**, 028101 (2015).
[29] S. Mahdisoltani, Riccardo Ben Alì Zinati, C. Duclut, A. Gambassi, and R. Golestanian, Nonequilibrium polarity-induced chemotaxis: Emergent Galilean symmetry and exact scaling exponents, Phys. Rev. Res. **3**, 013100 (2021).
[30] U. C. Täuber, *Critical Dynamics: A Field Theory Approach to Equilibrium and Non-Equilibrium Scaling Behavior* (Cambridge University Press, Cambridge, England, 2014), 10.1017/CBO9781139046213.
[31] E. O. Budrene and H. C. Berg, Complex patterns formed by motile cells of Escherichia coli, Nature (London) **349**, 630 (1991).
[32] L. Tweedy, D. A. Knecht, G. M. Mackay, and R. H. Insall, Self-generated chemoattractant gradients: Attractant

depletion extends the range and robustness of chemotaxis, PLoS Biol. **14**, e1002404 (2016).
[33] See Supplemental Material at http://link.aps.org/supplemental/10.1103/PhysRevLett.131.088201 for detailed calculations and technical background information, which includes Refs. [20,21,26,30,34–52].
[34] A. Cavagna, L. Di Carlo, I. Giardina, T. S. Grigera, S. Melillo, L. Parisi, G. Pisegna, and M. Scandolo, Natural swarms in 3.99 dimensions, Nat. Phys. (2023).
[35] L. Canet, H. Chaté, B. Delamotte, and N. Wschebor, Nonperturbative Renormalization Group for the Kardar-Parisi-Zhang Equation, Phys. Rev. Lett. **104**, 150601 (2010).
[36] N. Dupuis, L. Canet, A. Eichhorn, W. Metzner, J. M. Pawlowski, M. Tissier, and N. Wschebor, The nonperturbative functional renormalization group and its applications, Phys. Rep. **910**, 1 (2021).
[37] C. Gardiner, *Stochastic Methods: A Handbook for the Natural and Social Sciences*, Springer Series in Synergetics (Springer, Berlin Heidelberg, 2009).
[38] M. Doi, Second quantization representation for classical many-particle system, J. Phys. A **9**, 1465 (1976).
[39] L. Peliti, Path integral approach to birth-death processes on a lattice, J. Phys. France **46**, 1469 (1985).
[40] D. S. Dean, Langevin equation for the density of a system of interacting Langevin processes, J. Phys. A **29**, L613 (1996).
[41] K. Kawasaki, Stochastic model of slow dynamics in supercooled liquids and dense colloidal suspensions, Physica (Amsterdam) **208A**, 35 (1994).
[42] F. Caballero, C. Nardini, and M. E. Cates, From bulk to microphase separation in scalar active matter: A perturbative renormalization group analysis, J. Stat. Mech. (2018) 123208.
[43] M. Kardar, *Statistical Physics of Fields* (Cambridge University Press, Cambridge, England, 2007), 10.1017/CBO9780511815881.
[44] R. Bausch, H. K. Janssen, and H. Wagner, Renormalized field theory of critical dynamics, Z. Phys. B Condens. Matter **24**, 113 (1976).
[45] H. K. Janssen, On a Lagrangean for classical field dynamics and renormalization group calculations of dynamical critical properties, Z. Phys. B Condens. Matter **23**, 377 (1976).
[46] C. de Dominicis, Techniques de renormalisation de la theorie des champs et dynamique des phenomenes critques, J. Phys. (Paris), Colloq. **37**, 247 (1976).
[47] P. C. Martin, E. D. Siggia, and H. A. Rose, Statistical dynamics of classical systems, Phys. Rev. A **8**, 423 (1973).
[48] R. Mesibov, G. W. Ordal, and J. Adler, The range of attractant concentrations for bacterial chemotaxis and the threshold and size of response over this range, J. Gen. Physiol. **62**, 203 (1973).
[49] J. Zinn-Justin, *Quantum Field Theory and Critical Phenomena* (Oxford University Press, New York, 2002), 10.1093/acprof:oso/9780198509233.001.0001.
[50] H. K. Janssen, Survival and percolation probabilities in the field theory of growth models, J. Phys. Condens. Matter **17**, S1973 (2005).
[51] H. P. Langtangen and A. Logg, *Solving PDEs in* PYTHON (Springer, New York, 2017), 10.1007/978-3-319-52462-7.
[52] A. Logg and G. N. Wells, DOLFIN: Automated finite element computing, ACM Trans. Math. Softw. **37**, 1731030 (2010).
[53] R. A. Fisher, The wave of advance of advantageous genes, Ann. Eugen. **7**, 355 (1937).
[54] A. Kolmogorov, I. Petrovsky, and M. Piskunov, A study of the diffusion equation with increase in the amount of substance, and its application to a biological problem, Moscow Univ. Bull. Math. **1**, 1 (1937).
[55] L. A. Segel, A theoretical study of receptor mechanisms in bacterial chemotaxis, SIAM J. Appl. Math. **32**, 653 (1977).
[56] K. J. Painter and T. Hillen, Volume-filling and quorum-sensing in models for chemosensitive movement, Can. Appl. Math. Q. **10**, 501 (2002).
[57] A. Turing, The chemical basis of morphogenesis, Phil. Trans. R. Soc. B **237**, 37 (1952).
[58] P. Lewus and R. M. Ford, Quantification of random motility and chemotaxis bacterial transport coefficients using individual-cell and population-scale assays, Biotechnol. Bioeng. **75**, 292 (2001).
[59] J. D. Murray, *Mathematical Biology* (Springer, New York, 2003), 10.1007/b98868.
[60] E. Frey and U. C. Täuber, Two-loop renormalization-group analysis of the Burgers-Kardar-Parisi-Zhang equation, Phys. Rev. E **50**, 1024 (1994).
[61] H. K. Janssen, U. C. Täuber, and E. Frey, Exact results for the Kardar-Parisi-Zhang equation with spatially correlated noise, Eur. Phys. J. B **9**, 491 (1999).